11th World Congress on Computational Mechanics (WCCM XI)
5th European Conference on Computational Mechanics (ECCM V)
6th European Conference on Computational Fluid Dynamics (ECFD VI)
E. Oñate, J. Oliver and A. Huerta (Eds)

NUMERICAL SIMULATION OF ONE-DIMENSIONAL FLOW IN ELASTIC AND VISCOELASTIC BRANCHING TUBE

IVAN KORADE, ZDRAVKO VIRAG AND MARIO ŠAVAR

University of Zagreb, Faculty of Mechanical Engineering and Naval Architecture
Ivana Lučića 5, 10000 Zagreb, Croatia
email: ivan.korade@fsb.hr, zdravko.virag@fsb.hr, mario.savar@fsb.hr

Key Words: *Hemodynamics, Method of Characteristics, Unsteady Flow.*

Abstract. A method of characteristics for solving one-dimensional model of fluid flow in pipe networks with tree-like structure is developed. The method is validated in the case of flow with no wave reflections where the analytical solution is known. The method is applied to the fluid flow in a branching tube in cases of pure elastic and viscoelastic wall. The effects of wall stiffening and tube tapering were investigated. It is concluded that neither stiffening nor tapering can cause the effect of pressure wave steepening toward the periphery.

1 INTRODUCTION

Numerical simulation of blood flow in arterial tree is challenging, due to the difficulties in describing the geometry, nonlinear wall viscoelasticity, and non-Newtonian rheological properties of blood. One-dimensional models present a good compromise between Windkessel and three-dimensional models [1, 2]. Numerical simulation of arterial flow is very useful for the thorough understanding of pressure and flow waves propagation phenomena. Mathematical models differ in the modeling of friction term and constitutive relationship for the arterial wall. The simplest models use: (i) for friction, Hagen-Poiseuille law which is valid for the steady state flow; (ii) for arterial wall, the pure elastic model; and (iii) neglect the nonlinear convection term in the momentum equation. Such simplified, linear models may be reduced to the transmission line models and they are usually solved in the frequency domain. When nonlinearities are included into the model, it should be solved numerically in time domain. Method of characteristics is a natural numerical method for solving wave propagation in elastic pipes, although the finite difference, finite volume and finite element methods are also used.

The goal of this paper is to develop a method of characteristics for solving a nonlinear one-dimensional model in a branching tube with an elastic and viscoelastic wall. The proposed method will be tested in the case of reflectionless tube. The influence of the viscous resistance of the tube wall will be estimated by comparison of the results obtained for the pure elastic and viscoelastic tube. Also the effect of tube wall stiffening and tube tapering on the pressure wave steepening will be analyzed.

2 MATHEMATICAL MODEL

One-dimensional model of blood flow in a pipe with viscoelastic wall reads [3]:

$$\frac{\partial A}{\partial t}+\frac{\partial Q}{\partial x}=0 \tag{1}$$

$$\frac{\partial Q}{\partial t}+\frac{A}{\rho}\frac{\partial p}{\partial x}+\frac{\partial (Qv)}{\partial x}=-fQ \tag{2}$$

$$p-p_0=\frac{1}{C}(A-A_0)+\eta\frac{\partial A}{\partial t} \tag{3}$$

where x, t are the space and the time coordinate, respectively, A is the cross-sectional area ($A=D^2\pi/4$), Q is the volume flow rate, and $v=Q/A$, C is the areal compliance of the wall ($C=\mathrm{d}A/\mathrm{d}p$), η is the viscous resistance of the wall, ρ is the fluid density, and f is the friction coefficient. A_0 is the constant cross-sectional area at constant pressure p_0.

For the friction coefficient we use Hagen-Poiuseuille law for the steady state flow, which gives:

$$f=\frac{32\mu}{\rho D^2} \tag{4}$$

where μ is the fluid viscosity.

3 NUMERICAL METHOD

The artery is discretized into a number of elements of length Δx. Fig. 1 shows two typical elements (denoted by j and k) bounded by nodes (I, J, and K). The pressure is defined at the nodes, A is defined in the middle of each element (and it is considered to be constant along the element) and Q is defined at each end of each element. Thus, four unknowns are stored for each element. For example, the unknowns related to the element j are p_j, Q_jL, Q_jD and A_j, as shown in Fig. 1.

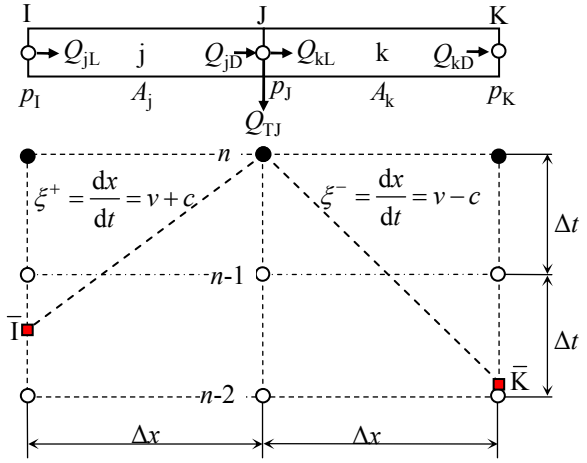

Figure 1: A part of discretized tube with arrangement of variables. Squares denote interpolation points.

Equations (1) to (3) may be transformed into ordinary differential equations that are valid along characteristics C^+ and C^- defined by $\xi^+ = dx/dt = v + c$ and $\xi^- = dx/dt = v - c$, in the form:

$$\frac{A}{\rho}dp + \xi^{\pm}dQ - v^2 dA = -fQ\Delta x - \eta\frac{A}{\rho}\frac{\partial^2 Q}{\partial x \partial t}dt \tag{5}$$

where $c = \sqrt{A/(\rho C)}$ is the wave speed. Along the third characteristic C^0 (applied for each element), defined by $\xi^0 = dx/dt = 0$, the following relationship holds:

$$dp - \frac{1}{C}dA = -\eta\frac{\partial^2 Q}{\partial x \partial t}dt \tag{6}$$

The fourth equation, related to each node, is the continuity equation. For example, at node J this equation reads:

$$Q_{jD} = Q_{kL} + Q_{TJ} \tag{7}$$

where Q_{TJ} is the transversal blood flow (the branching flow from the large artery into a small one). In each node, Q_{TJ} is modeled by the inertial four element Windkessel as depicted in Fig. 2. In this model, L_J is the inertance, r_J is the resistance, C_{TJ} is the capacity of branching arteries and R_J is the peripheral resistance at node J. Differential equation of this model is:

$$p_J + C_{TJ}R_J\frac{dp_J}{dt} = (R_J + r_J)Q_{TJ} + (C_{TJ}r_J R_J + L_J)\frac{dQ_{TJ}}{dt} + L_J C_{TJ} R_J \frac{d^2 Q_{TJ}}{dt^2} \tag{8}$$

We discretized equation (8) by applying a second order formula that uses the values of p_J and Q_{TJ} from three old time steps, and the final relationship between p_J and Q_{TJ} at the new time instant n, where a_{TJ} and b_{TJ} are coefficients that can be easily calculated.

Equations (5) and (6) are discretized by replacing differentials with finite differences, e.g. for pressure along the ξ^+ characteristic: $dp = p_J^n - \overline{p}_I$, and along ξ^+ characteristic: $dp = p_J^n - \overline{p}_K$. Fig. 3 illustrates the interpolation practice along C^+ defined by $dx/dt = v + c$. It is known that the explicit method of characteristics is stable when the Courant number $Co = (v + c)\Delta t/\Delta x$ is less or equal to 1 (see points B, C and D in Fig 3). When Co is greater than 1 (see point A in Fig. 3) we apply the time linear interpolation at node I between values in instances n and n-1. In that way the method retains stability, but becomes implicit. Since the proposed method is already implicit due to viscous resistance of arterial wall, it is acceptable to have Courant number greater than 1. Of course, it is known that the accuracy of the results decreases when Co number increases above 1, so it is recommended to keep it less than 1. In the proposed method, it is necessary to keep the values of variables from several old time steps. Normally, we apply linear time interpolation at node I, between two successive instances (see points B and C in Fig. 3). If the Courant number is so small that the characteristic line intersects the oldest saved time step (see point D in Fig. 3), the linear space interpolation is applied between nodes I and J in the oldest saved instant. Generally, the interpolated values may be defined by the following expressions:

$$\overline{p}_{\mathrm{I}} = a_{\mathrm{j+}} p_{\mathrm{I}} + b_{p\mathrm{j+}} \ , \ \overline{Q}_{\mathrm{j+}} = a_{\mathrm{j+}} Q_{\mathrm{jL}} + b_{Q\mathrm{j+}} \ \text{ and } \ \overline{A}_{\mathrm{j+}} = a_{\mathrm{j+}} A_{\mathrm{j}} + b_{A\mathrm{j+}} \tag{9}$$

where the interpolation factor $a_{\mathrm{j+}}$ takes a nonzero value only if Co>1. The analogue expressions are valid for the interpolation along the characteristic C$^-$.

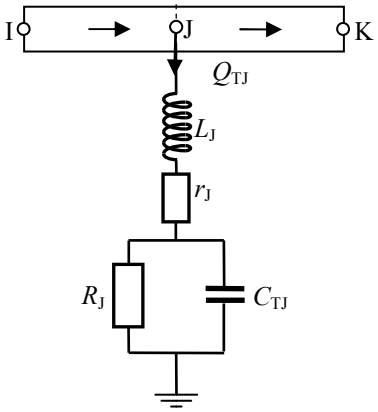

Figure 2: Electrical analogue scheme of the Windkessel model which defines Q_{T} from p_{J}

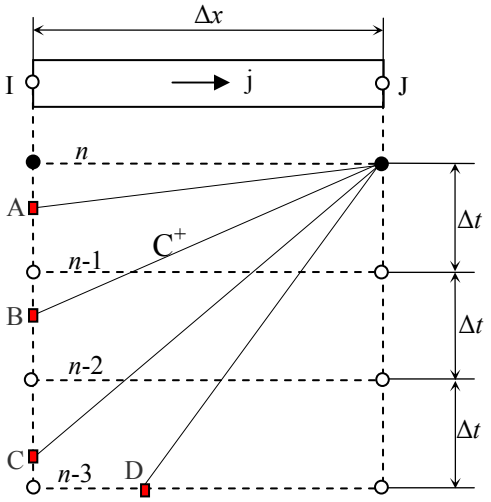

Figure 3: Interpolation practice along C$^+$ characteristics

To obtain a linear system of equations, all coefficients in equations (5) and (6) are discretized using the known variable values from the previous instance (n-1). The part of the source term related to the viscous resistance of the wall is discretized as (in all discretized equations that follow we will omit the superscript n – denoting the values from current instance, and superscript n-1 will be replaced by o):

$$\eta \frac{\partial^2 Q}{\partial x \partial t} \mathrm{d}t = \eta \left[\frac{Q_{\mathrm{jD}} - Q_{\mathrm{jL}}}{\Delta \mathrm{x}_{\mathrm{j}}} - \frac{Q^{\mathrm{o}}_{\mathrm{jD}} - Q^{\mathrm{o}}_{\mathrm{jL}}}{\Delta \mathrm{x}_{\mathrm{j}}} \right] \tag{10}$$

For the element j, the discretized form of equation (5) along C$^+$ is:

$$\frac{A^{\mathrm{o}}_{\mathrm{j}}}{\rho}\left(p_{\mathrm{J}} - \overline{p}_{\mathrm{I}}\right) + \left(v^{\mathrm{o}}_{\mathrm{j}} + c^{\mathrm{o}}_{\mathrm{j}}\right)\left(Q_{\mathrm{jD}} - \overline{Q}_{\mathrm{j+}}\right) - \left(v^{\mathrm{o}}_{\mathrm{j}}\right)^2 \left(A_{\mathrm{j}} - \overline{A}_{\mathrm{j+}}\right) = -f^{\mathrm{o}}_{\mathrm{j}} \left(\frac{Q_{\mathrm{jD}} + \overline{Q}_{\mathrm{j+}}}{2} \right) \Delta x_{\mathrm{j}} - \eta_{\mathrm{j}} \frac{A^{\mathrm{o}}_{\mathrm{j}}}{\rho} \frac{\partial^2 Q}{\partial x \partial t} \Delta t \tag{11}$$

and along C$^-$:

$$\frac{A^{\mathrm{o}}_{\mathrm{j}}}{\rho}\left(p_{\mathrm{I}} - \overline{p}_{\mathrm{J}}\right) + \left(v^{\mathrm{o}}_{\mathrm{j}} - c^{\mathrm{o}}_{\mathrm{j}}\right)\left(Q_{\mathrm{jL}} - \overline{Q}_{\mathrm{j-}}\right) - \left(v^{\mathrm{o}}_{\mathrm{j}}\right)^2 \left(A_{\mathrm{j}} - \overline{A}_{\mathrm{j-}}\right) = f^{\mathrm{o}}_{\mathrm{j}} \left(\frac{Q_{\mathrm{jL}} + \overline{Q}_{\mathrm{j-}}}{2} \right) \Delta x_{\mathrm{j}} - \eta_{\mathrm{j}} \frac{A^{\mathrm{o}}_{\mathrm{j}}}{\rho} \frac{\partial^2 Q}{\partial x \partial t} \Delta t \tag{12}$$

From equation (6), it follows for the element j:

$$\frac{p_{\mathrm{I}}+p_{\mathrm{J}}}{2}-\frac{p_{\mathrm{I}}^{\mathrm{o}}+p_{\mathrm{J}}^{\mathrm{o}}}{2}-\frac{1}{C_A}\left(A_{\mathrm{j}}-A_{\mathrm{j}}^{\mathrm{o}}\right)=-\eta_{\mathrm{j}}\left(\frac{Q_{\mathrm{jD}}-Q_{\mathrm{jL}}}{\Delta x_{\mathrm{j}}}-\frac{Q_{\mathrm{jD}}^{\mathrm{o}}-Q_{\mathrm{jL}}^{\mathrm{o}}}{\Delta x_{\mathrm{j}}}\right) \tag{13}$$

When applying equations (7) and (11) to (13) to all elements, the system of linear algebraic equations arise. One row of this system, written in the matrix form reads:

$$\underbrace{\begin{bmatrix} 0 & 0 & 0 & 0 \\ C_{21} & 0 & 0 & 0 \\ C_{31} & 0 & 0 & 0 \\ 0.5 & 0 & 0 & 0 \end{bmatrix}}_{\mathbf{C}^{\mathrm{j}}} \underbrace{\begin{bmatrix} p_{\mathrm{I}} \\ Q_{\mathrm{iL}} \\ Q_{\mathrm{iD}} \\ A_{\mathrm{i}} \end{bmatrix}}_{\mathbf{X}_{\mathrm{i}}} + \underbrace{\begin{bmatrix} A_{11} & 0 & 1 & 0 \\ A_{21} & A_{22} & A_{23} & A_{24} \\ A_{31} & A_{32} & A_{33} & A_{34} \\ 0.5 & A_{42} & A_{43} & A_{44} \end{bmatrix}}_{\mathbf{A}^{\mathrm{j}}} \underbrace{\begin{bmatrix} p_{\mathrm{J}} \\ Q_{\mathrm{jL}} \\ Q_{\mathrm{jD}} \\ A_{\mathrm{j}} \end{bmatrix}}_{\mathbf{X}_{\mathrm{j}}} + \underbrace{\begin{bmatrix} 0 & -1 & 0 & 0 \\ 0 & 0 & 0 & 0 \\ 0 & 0 & 0 & 0 \\ 0 & 0 & 0 & 0 \end{bmatrix}}_{\mathbf{B}^{\mathrm{j}}} \underbrace{\begin{bmatrix} p_{\mathrm{K}} \\ Q_{\mathrm{kL}} \\ Q_{\mathrm{kD}} \\ A_{\mathrm{k}} \end{bmatrix}}_{\mathbf{X}_{\mathrm{k}}} = \underbrace{\begin{bmatrix} D_1 \\ D_2 \\ D_3 \\ D_4 \end{bmatrix}}_{\mathbf{D}^{\mathrm{j}}} \tag{14}$$

For any arterial network with a tree-like structure, an efficient direct solver for solving the system of linear algebraic equations may be constructed, which uses the procedure similar to the one for solving a system with tri-diagonal matrix. Boundary conditions (prescribed pressure or flow rate at the input node of the network) may be easily implemented through the modification of coefficients in matrices **A** and **D**.

4 RESULTS AND DISCUSION

The described method was applied to a branching tube schematically shown in Fig. 4.

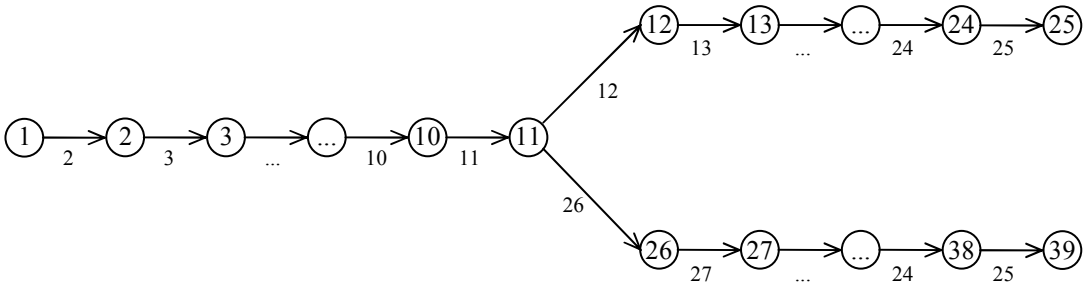

Figure 4: Scheme of the analyzed branching tube (the node numbers are encircled)

The branching tube is divided into 38 elements of length Δx=6 cm. The first 10 elements have a uniform cross section area A_0=5 cm^2 (at pressure p_0=0), and the cross-section area of each branching tube is $A_0/2$. The characteristic impedance of the mother vessel is $Z_0=\rho c/A_0$, and the characteristic impedance of the daughter vessels is two times greater. At the tube inlet (node 1), we prescribe the flow rate, and at the tube outlet (nodes 25 and 39), the peripheral resistances R_{25} and R_{39} are set. In all calculations, we consider two cases: a pure elastic (η=0), and a viscoelastic tube wall with η defined by the time constant $\tau=C\cdot\eta$ =C$\cdot Z_0/20$, where T is the period of the prescribed inflow. The input flow rate is designed as half sine wave at $T/3$ (T=0.3 s) of amplitude 50 ml/s. In all cases, the total integration time was 10T.

4.1 Test case (matching characteristic impedance and peripheral resistance)

We chose the terminal resistances R_{25}= R_{39}=2 mmHg·s/ml, the constant c=10 m/s, and ρ was selected to match $2R_{25}$ with characteristic impedance $Z_0 = \sqrt{\rho/(A_0 C)} = \rho c / A_0$. Fluid viscosity was zero and integration was performed at Co=1. Fig. 5 shows the results for the pure elastic wall, and it is obvious that the pressure and flow are in phase at each point of the tube, i.e. there are no wave reflections in the tube. Fig. 6 shows results for the viscoelastic wall ($\tau = C \cdot \eta$ =0.005). At the inlet node, the pressure is similar to the one obtained in the elastic tube, but there are great differences in flow rates and pressure profiles at distal nodes. This can be explained by wave reflections which are a consequence of arterial wall viscous resistance. It is interesting to note that an incisure appears in the inlet pressure profile, like in the real aortic root pressure. Also η causes the less steep pressure profile, which is opposite to the observations in the arterial tree.

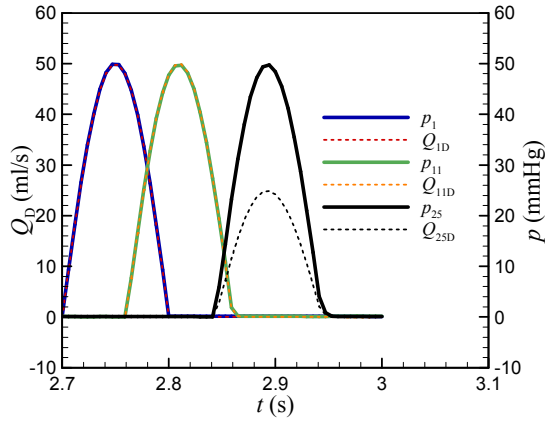

Figure 5: Results for pressure and flow rate at different locations for pure elastic tube with Z_0=$2R_{25}$

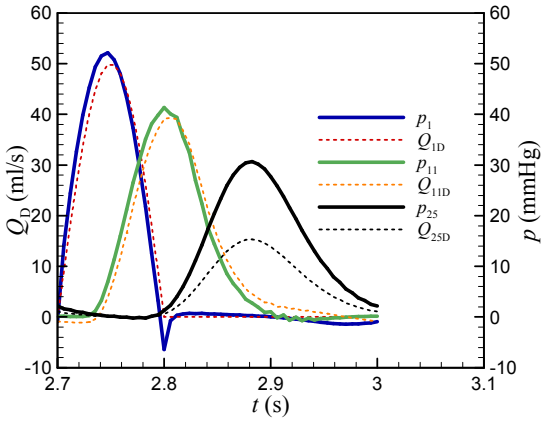

Figure 6: Results for pressure and flow rate at different locations for viscoelastic tube with Z_0=$2R_{25}$

4.2 Influence of wall stiffening with the distance from the inlet

In this test case, we introduced a variable tube compliance, by prescribing linearly varying wave velocity. At the inlet (element 2), c=4 m/s, at element 11, c=9. 4 m/s, at elements 12 and 26, c=10 m/s and at elements 25 and 39, c=17.8 m/s. Fluid viscosity was zero, and the integration time step was two times smaller than in the previous case. Fig. 7 and 8 show results for the pure elastic and viscoelastic wall, respectively. Due to the increased compliance at the tube inlet, the pressure is significantly lower than in the previous case. Obviously the viscous resistance increases the inlet pressure and decrese distal pressure with respect to the pure elastic case.

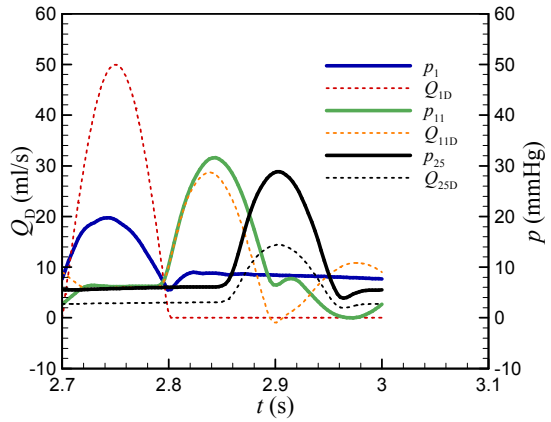

Figure 7: Results for pressure and flow rate at different locations for pure elastic tube with variable *c*

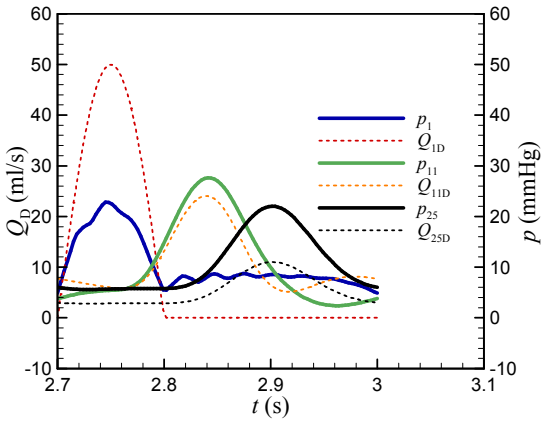

Figure 8: Results for pressure and flow rate at different locations for viscoelastic tube with variable *c*

4.3 Influence of the tube tapering

In this test case, we introduced the linearly varying tube diameter. The inlet diameter is 2.76 cm (area is about 6 cm^2), the parent tube has the diameter 2.29 cm (area is about 4.12 cm^2) at junction, while daughter tubes are 1.7 cm in diameter (area is 2.27 cm^2), and at the outlet diameter is 1.13 cm (area 1 cm^2). Fluid viscosity was zero and the integration was performed at *Co*=1. Since the wave speed is constant, the tube compliance is greater at the elements with greater diameter. This explains the fact that in pure elastic case (Fig. 9), the inlet pressure is less than the distal one, and the slope of the inlet pressure rise is small. In the case of viscoelastic wall, the inlet pressure rise is due to the viscous resistance of the wall.

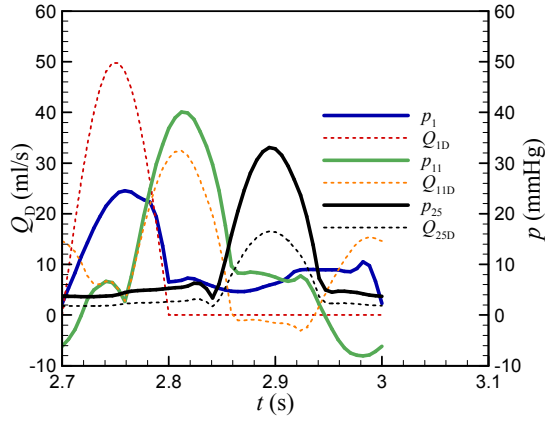

Figure 9: Results for pressure and flow rate at different locations for pure elastic tube with variable *D*

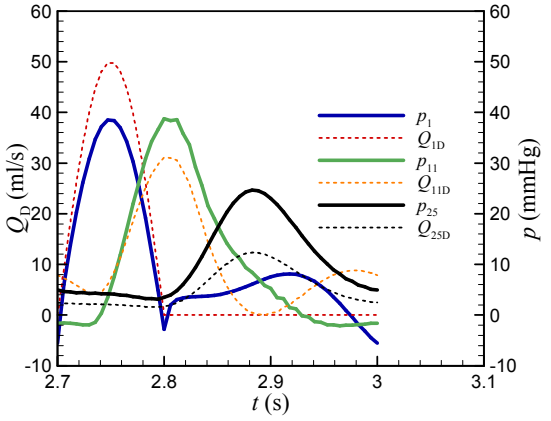

Figure 10: Results for pressure and flow rate at different locations for viscoelastic tube with variable *D*

5 CONCLUSIONS

- We proposed the method of characteristics for solving the one-dimensional model of fluid flow in a network of pure elastic or viscoelastic tubes with tree-like structure. In the case of viscoelastic tube, the proposed method is still physically clear and efficient, the same as in the case of an elastic tube.
- We applied the developed method to the branching tube, and analyzed the effects of pipe stiffening and tapering. In all analyzed cases, the stiffening and tapering do not cause the steepening of the pressure wave traveling towards the periphery, which exists in real circulatory systems.

REFERENCES

[1] Ottesen, J.T., Olufsen, M.S. and Larsen, J.K. *Applied mathematical models in human physiology*. BioMath-Group Department of Mathematics and Physics, Roskilde University, Denmark, (2003).

[2] van de Vosse, F.N. and Stergiopulos, N. Pulse Wave Propagation in the Arterial Tree. *Annu. Rev. Fluid Mech.* (2011), Vol **43**:467-99.

[3] Kitawaki, T. *Numerical Simulation Model with Viscoelasticity of Arterial Wall*. Chapter 9, http://dx.doi.org/10.5772/49976, (2012).